

Solutions of Maxwell's equations in presence of lamellar gratings including infinitely conducting metal

Boris Gralak,* Raphaël Pierre, Gérard Tayeb, and Stefan Enoch

Institut Fresnel-CNRS (UMR 6133), faculté de Saint Jérôme, 13397 Marseille cedex 20, France

**Corresponding author: boris.gralak@fresnel.fr*

Received June 16, 2008; revised September 18, 2008; accepted September 25, 2008;
posted October 13, 2008 (Doc. ID 97341); published November 25, 2008

Modal methods often used to model lamellar gratings that include infinitely or highly conducting metallic parts encounter numerical instabilities in some situations. In this paper, the origin of these numerical instabilities is determined, and then a stable algorithm solving this problem is proposed. In order to complete this analysis, the different geometries that can be handled without numerical instabilities are clearly defined. Numerical tests of the exact modal method implemented with the proposed solution are also presented. A test of convergence shows the efficiency of the method while the comparison with the fictitious sources method shows its accuracy. © 2008 Optical Society of America
OCIS codes: 050.2770, 050.1755.

1. INTRODUCTION

The exact ~~was~~ method was proposed in 1981 to solve Maxwell's equations in the presence of lamellar gratings [1–3]. This method relies on the expansion of the electromagnetic field using an “exact eigenfunctions basis” for which an exact representation of the permittivity is available. Consequently, it appears more efficient than the usual coupled-wave method [4] based on the use of a Fourier expansion that leads to poor convergence because of the discontinuous nature of both the electromagnetic field and the permittivity. When metallic materials are considered, the permittivity contrast is important, and the exact modal method is definitely a better alternative solution.

Motivations for studying lamellar metallic gratings are numerous. Periodic metallic structures are good candidates for extraordinary transmission [5,6], compact antennas [7], modified local density of states [8–10], negative index materials [11,12], etc. However, the use of the exact modal method (as well as the coupled-wave method) leads to numerical instabilities, even if *S* or *R* algorithms [13]—as well as modified *S* algorithms (also called the Fresnel formulation [14])—are implemented.

In this paper, we show how to obtain a large class of solutions of Maxwell's equations in the presence of lamellar gratings that include infinitely conducting metal. We extend the method presented in [15,16] in order to obtain a suitable model for metallic structures. We show that the numerical instabilities are due to a noninvertible matrix corresponding to the change from a first basis to a second basis, both with different supports. From our analysis, we show that the solution of this numerical problem is precisely the algorithm used in [17] whence we can define the structures that can be modeled without numerical instabilities. Finally, we present numerical examples to show that our solution is appropriate. A convergence test shows

that the method converges rapidly and is stable. In addition, a comparison of a field map with the fictitious-sources method shows perfect agreement.

2. DEFINITIONS AND NOTATIONS

In this paper, we show how to obtain solutions \mathbf{E}_ω of the Helmholtz equation

$$[\omega^2 - \epsilon^{-1} \nabla \times \mu_0^{-1} \nabla \times] \mathbf{E}_\omega = \mathbf{0}, \quad (1)$$

where $\nabla \times$ is the curl operator, ω is the frequency (real number), ϵ is the permittivity and μ_0 is the vacuum permeability. The function ϵ is well-defined for linear (eventually dispersive and absorptive) dielectric materials, and, in domains with infinitely conducting metal, the electric field is null. In order to obtain a first-order differential equation from Eq. (1), we define

$$\mathbf{H}_\omega = (\omega \mu_0)^{-1} \nabla \times \mathbf{E}_\omega. \quad (2)$$

Equation (1) is then equivalent to the set of first-order equations

$$\mathbf{E}_\omega = (\omega \epsilon)^{-1} \nabla \times \mathbf{H}_\omega, \quad \mathbf{H}_\omega = (\omega \mu_0)^{-1} \nabla \times \mathbf{E}_\omega. \quad (3)$$

If \mathbf{E}_ω stands for the harmonic electric field, the quantity \mathbf{H}_ω is then proportional to the usual harmonic magnetic field (the coefficient being the complex number i).

While Eqs. (1) and (3) are satisfied in linear dielectric materials only, the definition of the magnetic field (2) is satisfied everywhere. We can compile these two different behaviors by defining the characteristic function

$$\Psi = \begin{cases} 1 & \text{in dielectric materials} \\ 0 & \text{in infinitely conducting metal} \end{cases}. \quad (4)$$

Thus, the equations we propose to solve can be reduced to

$$\mathbf{E}_\omega = \Psi(\omega\epsilon)^{-1} \nabla \times \mathbf{H}_\omega, \quad \mathbf{H}_\omega = (\omega\mu_0)^{-1} \nabla \times \mathbf{E}_\omega. \quad (5)$$

Concerning the geometry, we focus on lamellar gratings that include infinitely conducting metal. Throughout, an orthonormal basis $(\mathbf{e}_1, \mathbf{e}_2, \mathbf{e}_3)$ is used, such that every vector \mathbf{x} in \mathbb{R}^3 is described by its three components x_1, x_2, x_3 . The structure we consider is independent of the variable x_2 , periodic with respect to the variable x_1 , and with spatial period $\mathbf{d} = d\mathbf{e}_1$:

$$\epsilon(\mathbf{x} + \mathbf{d}) = \epsilon(\mathbf{x}) = \epsilon(x_1, x_3), \quad \mathbf{x} \in \mathbb{R}^3. \quad (6)$$

The unit cell associated with this grating is $[0, d]$ and the one-dimensional lattice is $\{n\mathbf{d} | n \in \mathbb{Z}\}$. Then, a lamellar grating is a stack in the direction x_3 of layers in which ϵ is a function of the single variable x_1 (see Fig. 1). In practice, each layer comprises infinite parallel rods with rectangular cross section (see Fig. 2): the function ϵ is piecewise constant.

The exact modal method for solving Maxwell's equations in lamellar gratings made of dielectrics is already detailed in our previous paper [16]. In this paper, in a first step, each layer is considered separately and, at the end of this first step, we obtain an elementary R matrix associated with each layer. In a second step, an R matrix associated with a stack of layers is obtained from the R algorithm [13] and all the elementary R matrices.

Similarly, in the present paper we focus, in a first step, on a single layer that includes infinitely conducting metal. From [16], it is enough to obtain the elementary R matrix associated with such a layer. For the sake of simplicity, we first consider a layer made of two rods per unit cell similar to the one represented on Fig. 2: it is located between the two horizontal planes defined by equations $x_3 = 0$ and $x_3 = h$. The first rod is made of dielectric material with dielectric constant ϵ_a and width a , and the second rod is made of infinitely conducting metal (its width is $d - a$). Thus, defining the characteristic function

$$\Psi_a(x_1) = \begin{cases} 1 & 0 \leq x_1 + pd \leq a \\ 0 & a < x_1 + pd < d \end{cases}, \quad p \in \mathbb{Z}, \quad (7)$$

Eqs. (5) restricted to the domain $0 \leq x_3 \leq h$ become

$$\mathbf{E}_\omega = \Psi_a(\omega\epsilon_a)^{-1} \nabla \times \mathbf{H}_\omega, \quad \mathbf{H}_\omega = (\omega\mu_0)^{-1} \nabla \times \mathbf{E}_\omega. \quad (8)$$

In Appendix A, it is shown that we can restrict ourselves to an electromagnetic field $\mathbf{G}_\omega = \mathbf{E}_\omega, \mathbf{H}_\omega$ that satisfies the partial Bloch boundary condition

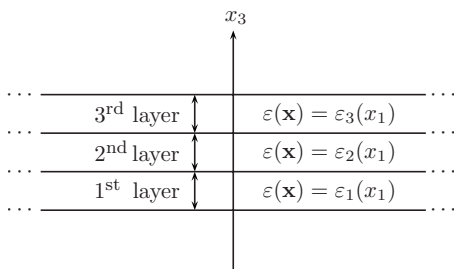


Fig. 1. Lamellar grating made of three layers.

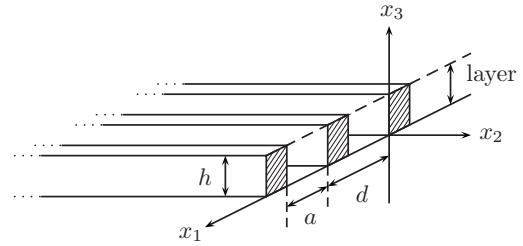


Fig. 2. Layer made of two rods per unit cell. First rod has width a and dielectric constant ϵ_a . Second rod (shaded domain) has width $d - a$ and is made of infinitely conducting metal; thickness of the layer is h .

$$\mathbf{G}_\omega(x_1 + d, x_2, x_3) = \exp[ik_1 d] \mathbf{G}_\omega(x_1, x_2, x_3), \quad (9)$$

$$x_1, k_1, x_2, x_3 \in \mathbb{R}$$

with the x_2 dependence

$$\mathbf{G}_\omega(x_1, x_2, x_3) = \hat{\mathbf{G}}_\omega(x_1, k_2, x_3) \exp[ik_2 x_2], \quad (10)$$

$$x_1, x_2, k_2, x_3 \in \mathbb{R}.$$

The resulting reduced unknowns $\hat{\mathbf{E}}_\omega$ and $\hat{\mathbf{H}}_\omega$ are, for all x_3 in \mathbb{R} , elements of the Hilbert space $\mathcal{H}(k_1)$, the space of square integrable functions on the domain $[0, d]$ of Eq. (A5) with the partial Bloch boundary condition (9).

3. TRANSFER MATRIX METHOD

In the following presentation of our numerical method, we will often use two- and four-component vectors (and then 2×2 and 4×4 matrices) in order to obtain compact notations containing all the electromagnetic field components which have to be taken into account.

The considered transfer matrix formalism is associated with the propagation variable x_3 [16]. In this formalism, the vector containing the tangential components of the reduced unknowns $\hat{\mathbf{E}}_\omega$ and $\hat{\mathbf{H}}_\omega$,

$$F = \begin{bmatrix} F^{(1)} \\ F^{(2)} \end{bmatrix}, \quad F^{(j)} = \begin{bmatrix} \hat{E}_{\omega,j} \\ \hat{H}_{\omega,j} \end{bmatrix}, \quad j = 1, 2, \quad (11)$$

is considered a function of the variable x_3 . As a consequence, although this vector-valued function F depends on the two variables x_1 and x_3 , the x_1 dependence will not appear in the following equations.

To allow focus on the main result of this paper, we report in Appendix B the details leading to the solution in the considered layer of Fig. 2. In particular, the modal basis $\{\Phi_{a,n} | n \in \mathbb{N}\}$ is determined by Eq. (B9) in order to obtain the modal expansion of the field

$$F(x_3) = \sum_{n \in \mathbb{N}} F_{a,n}(x_3) \Phi_{a,n}, \quad (12)$$

where the coefficients $F_{a,n}(x_3)$ are given by Eq. (B12). From this expansion, the relationships between the vectors $F(0)$ and $F(h)$ can be expressed with transfer matrix (B17) or R matrix (B19). More stable numerically, the R matrix is then used in the corresponding stacking algorithm.

Now, suppose that there is a second homogeneous layer with $\epsilon = \epsilon_0$, $\mu = \mu_0$ and located between the planes $x_3 = h$ and $x_3 = h + h_0$ (see Fig. 3).

In Appendix C, we show how the electromagnetic field can be expanded in the Fourier basis $\{\Phi_{0,p} | p \in \mathbb{Z}\}$ [Eq. (C2)] in the homogeneous layer

$$F(x_3) = \sum_{p \in \mathbb{Z}} F_{0,p}(x_3) \Phi_{0,p}, \quad (13)$$

where the coefficients $F_{0,p}(x_3)$ are given by Eq. (C6). Similarly, from this expansion, the relationships between the vectors $F(h)$ and $F(h + h_0)$ can be expressed with R matrix (C8).

At this stage, if one uses the usual R algorithm to obtain the R matrix of the stack of the two layers, then numerical instabilities will appear. In Section 4, we present our analysis and solution of this problem.

4. FROM THE FOURIER BASIS TO THE MODAL BASIS

A. Field Continuity at the Interface Separating a Lamellar Layer from a Homogeneous One

The interface separating the two considered layers is located at $x_3 = h$ (Fig. 3). Just below this interface at $x_3 = h^-$, the electromagnetic field is expanded on the modal basis (12), and just above at $x_3 = h^+$, the field is expanded on the Fourier basis (13). Then the expression of the field continuity at this interface requires one to change the expansion basis from the modal basis to the Fourier basis.

Let E and H be the two-component vectors containing, respectively, the electric and magnetic part of the vector F : from Eq. (11),

$$E = P^E F, \quad P^E = \begin{bmatrix} 1 & 0 & 0 & 0 \\ 0 & 0 & 1 & 0 \end{bmatrix},$$

$$H = P^H F, \quad P^H = \begin{bmatrix} 0 & 1 & 0 & 0 \\ 0 & 0 & 0 & 1 \end{bmatrix}. \quad (14)$$

The “modal” and Fourier coefficients associated with these vectors are defined from those of F in Eqs. (12) and (13) [see Eq. (B12) in Appendix B and Eq. (C6) in Appendix C for more details of the definition of the coefficients of F]:

$$E_{a,n}(x_3) = P^E F_{a,n}(x_3), \quad H_{a,n}(x_3) = P^H F_{a,n}(x_3), \quad n \in \mathbb{N},$$

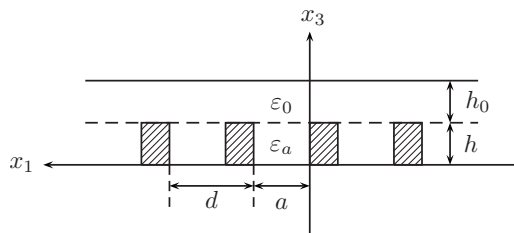


Fig. 3. Stack of a homogenous layer and the layer represented on Fig. 2. The interface delimiting these two layers is represented by the dashed line at $x_3 = h$.

$$E_{0,p}(x_3) = P^E F_{0,p}(x_3), \quad H_{0,p}(x_3) = P^H F_{0,p}(x_3), \quad p \in \mathbb{Z}. \quad (15)$$

Note that the “modal” coefficients are identified by the subscript a [see Eq. (12)] and the Fourier coefficients by the subscript 0 [see Eq. (13)]. These (two-component) coefficients are collected in the vectors E_0 , H_0 , E_a , and H_a representing the electric and magnetic components of the field F :

$$G_0(x_3) = [\cdots, G_{a,-1}(x_3), G_{a,0}(x_3), G_{a,1}(x_3), \cdots, G_{a,p}(x_3), \cdots],$$

$$G_a(x_3) = [G_{a,0}(x_3), G_{a,1}(x_3), \cdots, G_{a,n}(x_3), \cdots], \quad G = E, H. \quad (16)$$

From the continuity relationship established in Appendix A, the continuity condition at $x_3 = h$ can be written

$$E(x_1, h^-) = E(x_1, h^-) \Psi_a(x_1) = E(x_1, h^+),$$

$$H(x_1, h^-) \Psi_a(x_1) = H(x_1, h^+) \Psi_a(x_1), \quad 0 \leq x_1 \leq d. \quad (17)$$

After expanding the electromagnetic field on the modal [Eq. (B9)] and Fourier [Eq. (C2)] bases, this continuity condition becomes, for the coefficients in Eq. (15),

$$\sum_{n \in \mathbb{N}} \Phi_{a,n}^{(1)} E_{a,n}(h^-) = \Psi_a \sum_{n \in \mathbb{N}} \Phi_{a,n}^{(1)} E_{a,n}(h^-) = \sum_{p \in \mathbb{Z}} \phi_{0,p} E_{0,p}(h^+),$$

$$\Psi_a \sum_{n \in \mathbb{N}} \Phi_{a,n}^{(2)} H_{a,n}(h^-) = \Psi_a \sum_{p \in \mathbb{Z}} \phi_{0,p} H_{0,p}(h^+), \quad 0 \leq x_1 \leq d. \quad (18)$$

A priori we can use two different bases (the modal or the Fourier basis) to express this condition as a linear algebraic equation. However, the continuity of the electric field components implies a condition for all x_1 in $[0, d]$, while the continuity of the magnetic field components implies a condition for all x_1 in $[0, a]$ only. Consequently, the continuity of the electric field components has to be expressed by projection on the Fourier basis since the modal basis, cannot impose a condition for x_1 in $[a, d]$. On the other hand, the magnetic field components can be expressed using the Fourier basis as well as the modal basis. So, for the vectors E_0 , H_0 , E_a , and H_a in Eq. (16), these continuity conditions become

$$W_{0,a}^{(1)} E_a(h^-) = E_0(h^+),$$

$$W_{0,a}^{(2)} H_a(h^-) = U_a H_0(h^+) \Leftrightarrow H_a(h^-) = W_{a,0}^{(2)} H_0(h^+), \quad (19)$$

where $W_{0,a}^{(j)}$, $W_{a,0}^{(j)}$, and U_a are, respectively, the matrices with the 2×2 coefficients

$$[W_{0,a}^{(j)}]_{p,n} = \int_{[0,d]} dx_1 \overline{\phi_{0,p}(x_1)} \Phi_{a,n}^{(j)}(x_1),$$

$$p \in \mathbb{Z}, \quad n \in \mathbb{N}, \quad j = 1, 2,$$

$$[W_{a,0}^{(j)}]_{n,p} = \int_{[0,d]} dx_1 \Phi_{a,n}^{(j)}(x_1) \phi_{0,p}(x_1),$$

$$n \in \mathbb{N}, \quad p \in \mathbb{Z}, \quad j = 1, 2,$$

$$[U_a]_{p,q} = \int_{[0,d]} dx_1 \overline{\phi_{0,p}(x_1)} \Psi_a(x_1) \phi_{0,q}(x_1) I,$$

$$p \in \mathbb{Z}, \quad q \in \mathbb{Z}. \quad (20)$$

B. Origin of Numerical Instabilities

The difficulty of numerical instabilities arises from the fact that the set of plane-wave functions (C2) is a basis for functions on the interval $[0, d]$ while the sets of the modal functions (B3) and (B8) are bases for functions on the interval $[0, a]$. Consequently, it is possible to develop a modal function $\Phi_{a,n}$ on the set of the plane-wave functions $\Phi_{0,p}$, while the reverse is impossible. In practice (i.e., concerning numerical calculations), the matrices $W_{a,0}^{(j)}$, $W_{0,a}^{(j)}$, and U_a are not invertible (when truncated for numerical calculations).

For instance, consider the matrix $W_{a,0}^{(j)}$: it represents the basis functions $\varphi_{0,p} I$ expanded on the modal functions $\Phi_{a,n}^{(j)}$. After this expansion, the part of functions $\varphi_{0,p} I$ corresponding to the interval $[a, d]$ is equal to zero. In other words, this expansion of functions $\varphi_{0,p} I$ is associated with a projection leading to a development of functions $\Psi_a \varphi_{0,p} I$:

$$\sum_{n \in \mathbb{N}} [W_{a,0}^{(j)}]_{n,q} \Phi_{a,n}^{(j)} = \Psi_a \phi_{0,q} I \neq \phi_{0,q} I, \quad q \in \mathbb{Z}. \quad (21)$$

Now, if one applies the matrix $W_{0,a}^{(j)}$ to this matrix $W_{a,0}^{(j)}$, then one cannot recover the basis $\varphi_{0,p} I$ from the set of functions $\Psi_a \varphi_{0,p} I$. So, from Eq. (20), the product of (infinite) matrices $W_{0,a}^{(j)} W_{a,0}^{(j)}$ is not the identity for functions of the variable x_1 in $[0, d]$:

$$\sum_{p \in \mathbb{Z}} \sum_{n \in \mathbb{N}} [W_{0,a}^{(j)}]_{p,n} [W_{a,0}^{(j)}]_{n,q} \phi_{0,p} = \Psi_a \phi_{0,q} I \neq \phi_{0,q} I, \quad q \in \mathbb{Z},$$

$$\Leftrightarrow W_{0,a}^{(j)} W_{a,0}^{(j)} = U_a, \quad j = 1, 2. \quad (22)$$

Similarly, one can show that the product of (infinite) matrices $W_{a,0}^{(j)} W_{0,a}^{(j)}$ is the identity for functions of the variable x_1 in $[0, a]$:

$$\sum_{m \in \mathbb{N}} \sum_{p \in \mathbb{Z}} [W_{a,0}^{(j)}]_{m,p} [W_{0,a}^{(j)}]_{p,n} \Phi_{a,m}^{(j)} = \Phi_{a,n}^{(j)}, \quad n \in \mathbb{N},$$

$$\Leftrightarrow W_{a,0}^{(j)} W_{0,a}^{(j)} = I_a, \quad j = 1, 2, \quad (23)$$

where I_a is the infinite matrix with 2×2 coefficients

$$[I_a]_{m,n} = \begin{cases} I, & m = n \\ 0, & m \neq n \end{cases}, \quad m, n \in \mathbb{N}. \quad (24)$$

The two matrices U_a and I_a are actually the expressions of the projector associated with the function Ψ_a in two different bases (the plane-wave basis and the modal basis).

The two relationships (22) and (23) imply that the matrices $W_{a,0}^{(j)}$, $W_{0,a}^{(j)}$, and U_a are not invertible. Consequently,

the use of the R matrix (or S matrix) algorithm, which necessitates the inversion of these matrices [15,16], is associated with numerical instabilities.

C. Stable Numerical Method

We think that it is necessary to find a numerically stable technique to invert the matrices $W_{a,0}^{(j)}$, $W_{0,a}^{(j)}$, and U_a to avoid the use of the transfer matrices. The idea is that, if we add an invertible matrix I (B10) to a noninvertible matrix K , then the sum $[I+K]$ is in general invertible: for example, with the following 2×2 matrices, one has

$$K = \begin{bmatrix} 1 & 0 \\ 0 & 0 \end{bmatrix}, \quad [I+K]^{-1} = \begin{bmatrix} 2 & 0 \\ 0 & 1 \end{bmatrix}^{-1} = \begin{bmatrix} 1/2 & 0 \\ 0 & 1 \end{bmatrix}. \quad (25)$$

To use this idea, we define the ‘‘impedance’’ matrix Z_a associated with the layer of Fig. 2 by

$$\begin{bmatrix} E_a(h) \\ E_a(0) \end{bmatrix} = Z_a \begin{bmatrix} H_a(h) \\ H_a(0) \end{bmatrix}, \quad Z_a = \begin{bmatrix} Z_a^{(11)} & Z_a^{(12)} \\ Z_a^{(21)} & Z_a^{(22)} \end{bmatrix}. \quad (26)$$

This matrix is numerically stable and equivalent to the R matrix (B18). Indeed, the coefficients of the matrix Z_a can be deduced from the coefficients of the R matrix by identifying the expression (B18) with

$$\begin{bmatrix} E_{a,n}(h) \\ E_{a,n}(0) \end{bmatrix} = Z_{a,n} \begin{bmatrix} H_{a,n}(h) \\ H_{a,n}(0) \end{bmatrix}, \quad Z_{a,n} = \begin{bmatrix} Z_{a,n}^{(11)} & Z_{a,n}^{(12)} \\ Z_{a,n}^{(21)} & Z_{a,n}^{(22)} \end{bmatrix}, \quad n \in \mathbb{N}. \quad (27)$$

Similarly, we can define the ‘‘impedance’’ matrix Z_0 associated with the layer located between the planes $x_3 = h$ and $x_3 = h + h_0$ (Fig. 3) by

$$\begin{bmatrix} E_0(h_0 + h) \\ E_0(h) \end{bmatrix} = Z_0 \begin{bmatrix} H_0(h_0 + h) \\ H_0(h) \end{bmatrix}, \quad Z_0 = \begin{bmatrix} Z_0^{(11)} & Z_0^{(12)} \\ Z_0^{(21)} & Z_0^{(22)} \end{bmatrix}. \quad (28)$$

The expression of its coefficients $Z_{0,p}$ (p in \mathbb{Z}) can be deduced from the expression (C7) of the coefficients $R_{0,p}$ of the matrix R_0 .

The obtained ‘‘impedance’’ matrix Z_a is expressed in the modal basis while the matrix Z_0 is expressed in the Fourier basis. It is then necessary to use the continuity conditions (19) to obtain the impedance matrix associated with the two layers. To avoid ‘‘direct matrix inversion’’ we multiply $E_a(h)$ by $W_{0,a}^{(1)}$ and we replace $H_a(h)$ by $W_{a,0}^{(2)} H_0(h)$ in Eq. (26). Thus we obtain the relationship

$$\begin{bmatrix} E_a(h) \\ E_a(0) \end{bmatrix} = \tilde{Z}_a \begin{bmatrix} H_0(h) \\ H_a(0) \end{bmatrix}, \quad \tilde{Z}_a = \begin{bmatrix} W_{0,a}^{(1)} Z_a^{(11)} W_{a,0}^{(2)} & W_{0,a}^{(1)} Z_a^{(12)} \\ Z_a^{(21)} W_{a,0}^{(2)} & Z_a^{(22)} \end{bmatrix}. \quad (29)$$

This matrix \tilde{Z}_a is clearly obtained without numerical instabilities since it is based only on matrix multiplications.

Finally, let Z_{0a} be the impedance matrix associated with the stack made of the homogeneous layer and the layer containing infinitely conducting rods (Fig. 3):

$$\begin{bmatrix} E_0(h_0 + h) \\ E_a(0) \end{bmatrix} = Z_{0a} \begin{bmatrix} H_0(h_0 + h) \\ H_a(0) \end{bmatrix}. \quad (30)$$

This matrix can be expressed from the matrices Z_0 and \tilde{Z}_a with the group law \star defined in [13,16]: $Z_{0a} = Z_0 \star \tilde{Z}_a$. In particular, the elimination of $E_0(h)$ and $H_0(h)$ in Eqs. (28) and (29), shows that, to obtain Z_{0a} , the only matrix that has to be inverted is

$$Z_0^{(22)} - W_{0,a}^{(1)} Z_a^{(11)} W_{a,0}^{(2)}. \quad (31)$$

From our argument (25), and since $Z_0^{(22)}$ is invertible, this matrix is certainly invertible as well. Consequently, our numerical method is expected to be stable, and indeed, numerical results presented in Section 6 confirm this argument. Of course, this method is still valid if the matrix Z_0 is associated with a standard lamellar layer made of dielectric materials.

Note that in this particular case of a stack made of homogeneous layer and a layer containing infinitely conducting rods, we find that the solution for the interface at $x_3 = h$ is precisely the algorithm used in [17]. A similar procedure has to be realized for the interface at $x_3 = 0$ if the layer below is made of dielectric materials. In Section 5, we show that the solution we proposed can be extended to other geometries and, in particular, to geometries more complicated than the one already considered in the literature [17].

5. EXTENSION TO A STACK OF LAYERS CONTAINING INFINITELY CONDUCTING RODS

In this section, we show how to express without numerical instabilities the continuity condition at an interface separating two layers containing infinitely conducting rods.

A. Basic Example

We consider the structure represented on Fig. 4 with two adjacent layers containing infinitely conducting rods. The new layer is located between the two horizontal planes defined by equations $x_3 = 0$ and $x_3 = -h_b$. The first rod is made of dielectric material with dielectric constant ϵ_b and

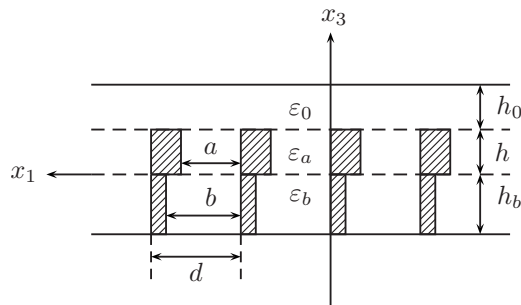


Fig. 4. Structure containing two adjacent layers with infinitely conducting rods. The bottom layer is made of two rods per unit cell: the first rod has width b and dielectric constant ϵ_b , the second rod (shaded domain) has width $d - b$ and is made of infinitely conducting metal; thickness of this layer is h_b .

width b , and the second rod is made of infinitely conducting metal (its width is $d - b$). Thus, the characteristic function of this layer is

$$\Psi_b(x_1) = \begin{cases} 1 & 0 \leq x_1 + pd \leq b \\ 0 & b < x_1 + pd < d \end{cases}, \quad p \in \mathbb{Z}. \quad (32)$$

Repeating what we did in Sections 3 and 4, we obtain the impedance matrix Z_b associated with the bottom layer:

$$\begin{bmatrix} E_b(0) \\ E_b(-h_b) \end{bmatrix} = Z_b \begin{bmatrix} H_b(0) \\ H_b(-h_b) \end{bmatrix}, \quad Z_b = \begin{bmatrix} Z_b^{(11)} & Z_b^{(12)} \\ Z_b^{(21)} & Z_b^{(22)} \end{bmatrix}. \quad (33)$$

This impedance matrix Z_b as well as the vectors $E_b(0)$, $E_b(-h_b)$, $H_b(0)$, and $H_b(-h_b)$ are expressed in the modal basis given by Eqs. (B9) and (B10), where all the subscripts a have been replaced by b .

From our analysis in Section 4, we know that it is necessary to express rigorously one modal basis ($\Phi_{a,n}^{(j)}$ or $\Phi_{b,n}^{(j)}$) using the second modal basis (respectively, $\Phi_{b,n}^{(j)}$ or $\Phi_{a,n}^{(j)}$). As represented on Fig. 4, suppose that

$$b \geq a \Leftrightarrow \Psi_a \Psi_b = \Psi_a; \quad (34)$$

then at the interface $x_3 = 0$, the modal basis $\Phi_{b,n}^{(j)}$ plays the same role as the Fourier basis at the interface $x_3 = h$, since it has the largest support. The continuity conditions at $x_3 = 0$ for the vectors E_a , H_a , E_b , and H_b should be written

$$\begin{aligned} W_{b,a}^{(1)} E_a(0^+) &= E_b(0^-), \\ H_a(0^+) &= W_{a,b}^{(2)} H_b(0^-), \end{aligned} \quad (35)$$

where $W_{b,a}^{(j)}$ and $W_{a,b}^{(j)}$ are, respectively, the matrices with the 2×2 coefficients

$$\begin{aligned} [W_{a,b}^{(j)}]_{m,n} &= [W_{b,a}^{(j)}]_{n,m} = \int_{[0,d]} dx_1 \Phi_{a,m}^{(j)}(x_1) \Phi_{b,n}^{(j)}(x_1), \\ m, n \in \mathbb{N}, \quad j &= 1, 2. \end{aligned} \quad (36)$$

Again, to avoid matrix inversion, these continuity conditions at $x_3 = 0$ have to be included in the matrix Z_a , which becomes

$$\begin{bmatrix} E_a(h) \\ E_b(0) \end{bmatrix} = \hat{Z}_a \begin{bmatrix} H_a(h) \\ H_b(0) \end{bmatrix}, \quad \hat{Z}_a = \begin{bmatrix} Z_a^{(11)} & Z_a^{(12)} W_{a,b}^{(2)} \\ W_{b,a}^{(1)} Z_a^{(21)} & W_{b,a}^{(1)} Z_a^{(22)} W_{a,b}^{(2)} \end{bmatrix}. \quad (37)$$

This matrix \hat{Z}_a can be combined (without numerical instabilities) with Z_b to obtain $Z_{ab} = \hat{Z}_a \star Z_b$, the impedance matrix associated with the layers a and b . Indeed, in this case, the only matrix that has to be inverted to obtain Z_{ab} is

$$W_{b,a}^{(1)} Z_a^{(22)} W_{a,b}^{(2)} - Z_b^{(11)}. \quad (38)$$

Note that it is possible to combine the continuity conditions at $x_3 = 0$ and $x_3 = h$ to define the matrix

$$\hat{Z}_a = \begin{bmatrix} W_{0,a}^{(1)} Z_a^{(11)} W_{a,0}^{(2)} & W_{0,a}^{(1)} Z_a^{(12)} W_{a,b}^{(2)} \\ W_{b,a}^{(1)} Z_a^{(21)} W_{a,0}^{(2)} & W_{b,a}^{(1)} Z_a^{(22)} W_{a,b}^{(2)} \end{bmatrix}. \quad (39)$$

This matrix can be combined (without numerical instabilities) with Z_b and Z_0 to obtain $Z_{0ab} = Z_0 \star \hat{Z}_a \star Z_b$, the impedance matrix associated with the three layers represented on Fig. 4.

Finally, in contrast to hypothesis (34), suppose that

$$a \geq b \Leftrightarrow \Psi_a \Psi_b = \Psi_b; \quad (40)$$

then, at the interface $x_3=0$ the modal basis $\Phi_{a,n}^{(j)}$ plays the same role as the Fourier basis at the interface $x_3=h$, since it has the largest support. The continuity conditions at $x_3=0$ for the vectors E_a, H_a, E_b , and H_b have to be written

$$E_a(0^+) = W_{a,b}^{(1)} E_b(0^-),$$

$$W_{b,a}^{(2)} H_a(0^+) = H_b(0^-), \quad (41)$$

where the expression of matrices $W_{b,a}^{(j)}$ and $W_{a,b}^{(j)}$ is given by Eq. (36). Thus these continuity conditions have to be included in the matrix Z_b , which becomes

$$\begin{bmatrix} E_a(0) \\ E_b(-h_b) \end{bmatrix} = \tilde{Z}_b \begin{bmatrix} H_b(0) \\ H_b(-h_b) \end{bmatrix},$$

$$\tilde{Z}_b = \begin{bmatrix} W_{b,a}^{(1)} Z_b^{(11)} W_{a,b}^{(2)} & W_{b,a}^{(1)} Z_b^{(12)} \\ Z_a^{(21)} W_{a,b}^{(2)} & Z_a^{(22)} \end{bmatrix}. \quad (42)$$

This matrix \tilde{Z}_b can be combined (without numerical instabilities) with Z_a to obtain $Z_{ab} = Z_a \star \tilde{Z}_b$, the impedance matrix associated with the layers a and b . Also, it is possible to combine this matrix with \tilde{Z}_a and then Z_0 to obtain $Z_{0ab} = Z_0 \star \tilde{Z}_a \star \tilde{Z}_b$ in the case of Eq. (40).

B. General Case

In the general case, a layer can contain several infinitely conducting rods (see Fig. 5). For example, to describe the top layer of Fig. 5, we define the characteristic function

$$\Psi_a = \Psi_{a_1} + \Psi_{a_2} + \dots + \Psi_{a_q},$$

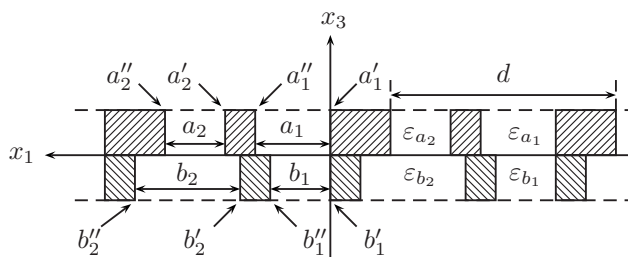


Fig. 5. Structure containing two adjacent layers with infinitely conducting rods. Each layer contains four different rods: the two dielectric rods have widths $c_1=c'_1-c'_2$ and $c_2=c''_2-c'_2$ and dielectric constants ϵ_{c_1} and ϵ_{c_2} ($c=a$ for the top layer and $c=b$ for the bottom layer). The other two rods (shaded domain) are made of infinitely conducting metal.

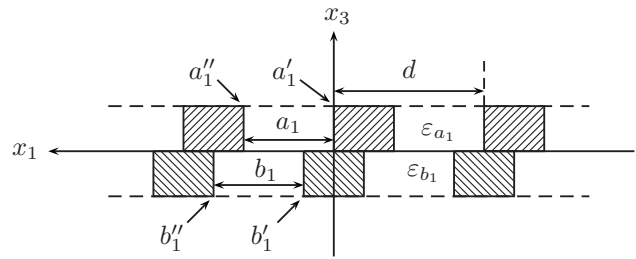


Fig. 6. Structure that cannot be modeled using a numerical stacking algorithm, since $a'_1 < b'_1 < a''_1 < b''_1$.

$$\Psi_{a_j} = \begin{cases} 1 & a'_j \leq x_1 + pd \leq a''_j \\ 0 & a''_j < x_1 + pd < a'_{j+1} \end{cases}, \quad p \in \mathbb{Z}, \quad (43)$$

from the parameter

$$a = (a'_1, a''_1, a'_2, a''_2, \dots, a'_q, a''_q, a'_{q+1}) \quad a'_{q+1} = d, \quad (44)$$

with $q=2$. Similarly, the bottom layer of Fig. 5 is described using the characteristic function

$$\Psi_b = \Psi_{b_1} + \Psi_{b_2} + \dots + \Psi_{b_l}, \quad (45)$$

with $l=2$.

All the calculations of Sections 3 and 4 can be realized for each dielectric rod corresponding to characteristic functions Ψ_{a_j} ($j=1, 2, \dots, q$) and Ψ_{b_k} ($k=1, 2, \dots, l$). From our analysis of Subsection 5.A, we can deduce that it is possible to obtain a stable stacking algorithm if, for each dielectric rod corresponding to Ψ_{a_j} ($j=1, 2, \dots, q$), there exists a rod with the corresponding Ψ_{b_k} (k in $\{1, 2, \dots, l\}$) such that

$$\Psi_{a_j} \Psi_{b_k} = \Psi_{a_j} \quad \text{or} \quad \Psi_{a_j} \Psi_{b_k} = \Psi_{b_k}. \quad (46)$$

In the case where $\Psi_{a_j} \Psi_{b_k} = \Psi_{a_j}$ (for example, $\Psi_{a_2} \Psi_{b_2} = \Psi_{a_2}$ in the case of Fig. 5), the procedure presented from relation (34) to equation (39) has to be used. And in the case $\Psi_{a_j} \Psi_{b_k} = \Psi_{b_k}$ (for example, $\Psi_{a_1} \Psi_{b_1} = \Psi_{b_1}$ in the case of Fig. 5), the procedure presented from relation (40) to equation (42) has to be used.

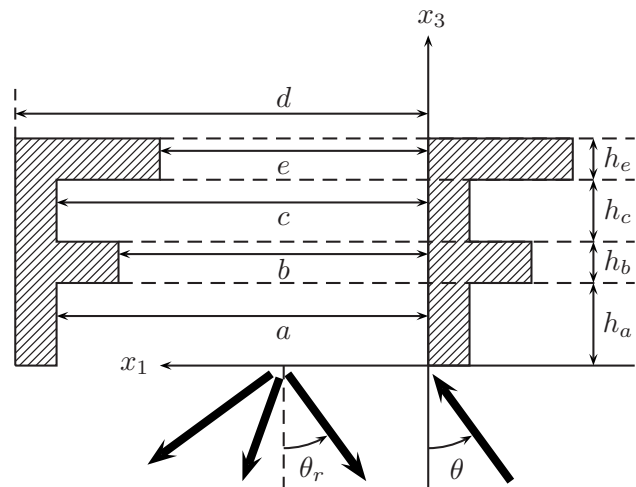


Fig. 7. Structure under consideration. The spatial period is $d=20.0$. The four layers have widths $a=18.0$, $b=15.0$, $c=18.0$, $e=13.0$, and thicknesses $h_a=4.0$, $h_b=2.0$, $h_c=3.0$, $h_e=2.0$.

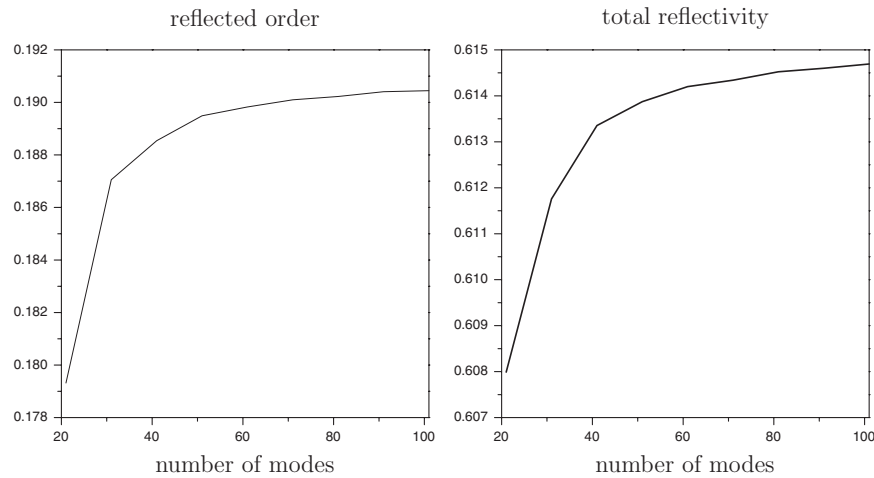


Fig. 8. Convergence of the main reflected order (left) and of the total reflectivity (right) when the number of modes is increasing.

Of course the condition (46) stays valid in the trivial case where the rod corresponding to Ψ_{a_j} has no connection with all the rods of the layer b (for example, $\Psi_{b_k} = 0$ if $b'_k = b''_k$). Thus it defines definitely the condition permitting the use of the stable numerical algorithm.

C. Limits of the Stable Numerical Method

We here define precisely the conditions where the algorithm we have defined cannot be used. These conditions are the negation of Eq. (46) so they can be written

$$\Psi_{a_j} \Psi_{b_k} \neq \Psi_{a_j}, \quad \Psi_{a_j} \Psi_{b_k} \neq \Psi_{b_k}, \quad \Psi_{a_j} \Psi_{b_k} \neq 0. \quad (47)$$

In practice, this condition corresponds to the example represented on Fig. 6.

6. NUMERICAL RESULTS

To show that our numerical procedure is numerically stable, we consider the ‘‘canonic’’ example defined in [18] and repeated on a one-dimensional lattice. The structure is then a set of periodically spaced and infinitely conducting F embedded in vacuum (see Fig. 7).

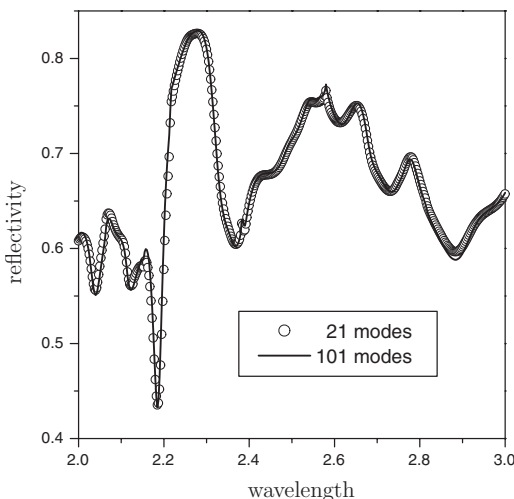


Fig. 9. Total reflectivity as a function of the wavelength (from 2.0 to 3.0) for two different numbers of modes.

This structure is illuminated by a plane wave with wavelength equal to $2.0 = 0.1d$, corresponding in this paper to the normalized frequency $\omega d \sqrt{\epsilon_0 \mu_0} / (2\pi) = 0.5$. The incident angle of this plane wave is $\theta = 45^\circ$, and the conical angle $\varphi = 30^\circ$. Thus, the incident wavevector $\mathbf{k}^i = k_1 \mathbf{e}_1 + k_2 \mathbf{e}_2 + k_3 \mathbf{e}_3$ is well defined since $k_1 = \omega \sqrt{\epsilon_0 \mu_0} \sin \theta \cos \phi$, $k_2 = \omega \sqrt{\epsilon_0 \mu_0} \sin \theta \sin \phi$, and $k_1^2 + k_2^2 + k_3^2 = \omega^2 \epsilon_0 \mu_0$. Finally, the incident field is *s*-polarized: the electric field is perpendicular to the incident plane, i.e., parallel to the vector $\mathbf{e}_s = k_2 \mathbf{e}_1 - k_1 \mathbf{e}_2$.

Figure 8 shows the reflected order with larger amplitude (for $\theta_r \approx \theta$ on Fig. 7, corresponding to $k_1 + p2\pi/d \approx -k_1$ with $p = -12$ for the first component of the reflected wave vector) and the total reflectivity as functions of the number of modes. It clearly shows that the algorithm is stable and convergent.

To complete this test of numerical stability, we have represented on Fig. 9 the total reflectivity as a function of the wavelength $2\pi / (\omega \sqrt{\epsilon_0 \mu_0})$ for 21 and 101 modes. The result shows that the exact modal method converges very rapidly since, for $2\pi / (\omega \sqrt{\epsilon_0 \mu_0})$ equal to 2.0 and 3.0, there are, respectively, 19 and 13 diffracted orders.

As a final word, we thought it would be relevant to compare our results to those obtained through another numerical method: the fictitious-sources method. The latter, described in [18–23], has the ability to solve problems of diffraction by arbitrarily shaped objects. Moreover, it is well adapted to perfectly conducting materials.

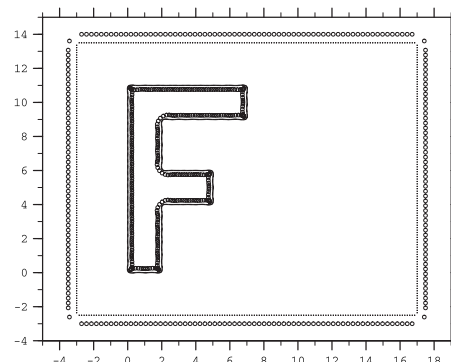


Fig. 10. Discretized objects (rectangular cell and the F). Black points and open circles fictitious sources represent.



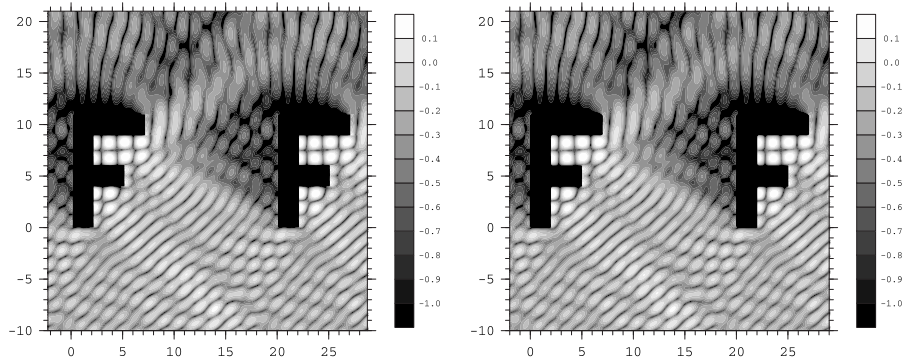


Fig. 11. Maps of $\log_{10}|E_1|$ —the electric field along the periodicity direction—using the modal method (left) and the fictitious-sources method (right).

In order to handle periodic geometries, diffractive objects are embedded in a cell—a rectangular fictitious object. Its width is the period d , its height is arbitrary (provided that the objects are entirely contained within the cell domain), and its edges have particular properties: the two vertical (lateral) edges are linked to each other thanks to periodic boundary conditions; the two horizontal edges are connected to surrounding media by Rayleigh expansions (heading upward from the topmost side and downward from the other one).

Getting back to our case, the electromagnetic field inside the cell (but outside the F) is fed by 300 fictitious sources located inside the F and 250 outside the cell (see Fig. 10 for the location of these sources). The boundary conditions are enforced using a least-squares algorithm with 600 points on the F and 500 on the cell. Above and below the cell, the electromagnetic field is expressed as a sum of 51 diffraction orders.

The calculations performed by the fictitious-sources method were more than 99% accurate regarding the energy balance criterion. To illustrate the comparison, we plot a map in the neighborhood of the structure using both methods (see Fig. 11).

Since the contour levels and scales are identical, one can compare the two maps of Fig. 11 and see that the agreement between the two methods is nearly perfect.

7. CONCLUSION

We have shown that by using the appropriate algorithm the exact modal method can be used to solve Maxwell's equations in presence of various kinds of lamellar grating that contain infinitely conducting metal. Note, moreover, that with a similar analysis, we can argue that the proposed method stays valid for highly conducting metallic parts. In that case, the only additional difficulty consists in finding the exact eigenvalues and eigenfunctions. A solution has been provided in [17] due to a perturbation theory. Also, it has to be noted that the presence of dielectric materials will not change the conclusions of the present paper.

The same stacking solution should be valuable if used in conjunction with the Fourier modal method also.

Finally, the analysis can be easily generalized to the case of three-dimensional structures. In particular, the

proposed algorithm should be stable in the case of such interesting structures as infinitely (or highly) conducting plates with holes.

APPENDIX A: ELECTROMAGNETIC FIELD

We assume only that the electromagnetic field satisfies the prerequisite finite energy criterion of square integrability in all horizontal planes:

$$\int_{\mathbb{R}^2} dx_1 dx_2 |\mathbf{G}_\omega(\mathbf{x})|^2 < \infty, \quad x_3 \in \mathbb{R}, \quad \mathbf{G}_\omega = \mathbf{E}_\omega, \mathbf{H}_\omega. \quad (\text{A1})$$

As a first consequence, it is possible to apply to Eqs. (8) a Fourier transform \mathcal{F}_0 with respect to the variable x_2 in order to take advantage of the x_2 invariance:

$$[\mathcal{F}_0(\mathbf{G}_\omega)](x_1, k_2, x_3) = \frac{1}{\sqrt{2\pi}} \int_{\mathbb{R}} dx_2 \exp(-ik_2 x_2) \mathbf{G}_\omega(x_1, x_2, x_3), \quad (\text{A2})$$

for all $x_1, k_2, x_3 \in \mathbb{R}$ and $\mathbf{G}_\omega = \mathbf{E}_\omega, \mathbf{H}_\omega$. The original solution is then recomposed by the inverse Fourier transform.

As a second consequence of Eq. (A1), it is possible to apply to Eqs. (8) a Floquet–Bloch transform \mathcal{F}_d with respect to the variable x_1 in order to take advantage of the x_1 periodicity:

$$[\mathcal{F}_d(\mathbf{G}_\omega)](x_1, k_1, x_2, x_3) = \sum_{p \in \mathbb{Z}} \mathbf{G}_\omega(x_1 + pd, x_2, x_3) \exp(-ik_1 pd), \quad (\text{A3})$$

for all $x_1, k_1, x_2, x_3 \in \mathbb{R}$ and $\mathbf{G}_\omega = \mathbf{E}_\omega, \mathbf{H}_\omega$. The original solution is then recomposed by the inverse Floquet–Bloch transform

$$\mathbf{G}_\omega(x_1, x_2, x_3) = \frac{d}{2\pi} \int_{(-\pi/d, \pi/d)} dk_1 [\mathcal{F}_d(\mathbf{G}_\omega)](x_1, k_1, x_2, x_3), \quad (\text{A4})$$

for all $x_1, x_2, x_3 \in \mathbb{R}$ and $\mathbf{G}_\omega = \mathbf{E}_\omega, \mathbf{H}_\omega$. After the application of these Fourier (A2) and Floquet–Bloch (A3) transforms, $\hat{\mathbf{G}}_\omega = \mathcal{F}_d[\mathcal{F}_0(\mathbf{G}_\omega)]$ satisfies for $\mathbf{G}_\omega = \mathbf{E}_\omega, \mathbf{H}_\omega$ the criterion

$$\int_{[0,d]} dx_1 |\hat{\mathbf{G}}_\omega(x_1, k_1, k_2, x_3)|^2 < \infty, \quad k_1, k_2, x_3 \in \mathbb{R}, \quad (\text{A5})$$

as well as the partial Bloch boundary condition

$$\begin{aligned} \hat{\mathbf{G}}_\omega(x_1 + d, k_1, k_2, x_3) &= \exp(ik_1 d) \hat{\mathbf{G}}_\omega(x_1, k_1, k_2, x_3), \\ x_1, k_1, k_2, x_3 &\in \mathbb{R}. \end{aligned} \quad (\text{A6})$$

Then Eq. (8) becomes

$$\hat{\mathbf{E}}_\omega = \Psi_a(\omega\epsilon_a)^{-1} \nabla_{k_2} \times \hat{\mathbf{H}}_\omega, \quad \hat{\mathbf{H}}_\omega = (\omega\mu_0)^{-1} \nabla_{k_2} \times \hat{\mathbf{E}}_\omega, \quad (\text{A7})$$

where $\nabla_{k_2} \times$ is the curl operator with the partial derivation ∂_2 replaced by ik_2 .

For all fixed Bloch wave vector k_1 , we denote by $\mathcal{H}(k_1)$ the Hilbert space of functions that satisfy the two conditions (A5) and (A6), i.e., the space square integrable function on the domain $[0, d]$ with the partial Bloch boundary condition.

As a third consequence, the combination of the square integrability of Eqs. (A1) and (A5) together with Eqs. (A8) below imposes that (1) the tangential components of $\hat{\mathbf{E}}_\omega$ are continuous at all the interfaces separating dielectrics and infinitely conducting metal [since $\hat{\mathbf{H}}_\omega = (\omega\mu_0)^{-1} \nabla \times \hat{\mathbf{E}}_\omega$ everywhere], and (2) the tangential components of $\hat{\mathbf{H}}_\omega$ are continuous at all the interfaces separating dielectrics. More precisely, in the present case, the metallic rod imposes the conditions

$$\begin{aligned} \hat{E}_{\omega,1}(x_1, k_1, k_2, x_3) &= \hat{E}_{\omega,2}(x_1, k_1, k_2, x_3) = 0, \\ a \leq x_1 \leq d, \quad x_3 &= 0, h; \end{aligned}$$

$$\begin{aligned} \hat{E}_{\omega,2}(x_1, k_1, k_2, x_3) &= \hat{E}_{\omega,3}(x_1, k_1, k_2, x_3) = 0, \\ 0 \leq x_3 \leq h, \quad x_1 &= 0, a. \end{aligned} \quad (\text{A8})$$

APPENDIX B: SOLUTION OF MAXWELL'S EQUATION IN A LAYER CONTAINING INFINITELY CONDUCTING METAL

1. Determination of the Modal Basis

From Eqs. (A7) and (A8), the components $\hat{E}_{\omega,2}$ and $\hat{E}_{\omega,3}$ of the electric field are continuous functions of the variable x_1 and satisfy the equation

$$(\partial_3^2 + L_a) \hat{E}_{\omega,j} = 0, \quad L_a = \omega^2 \epsilon_a \mu_0 - k_2^2 + \partial_1^2, \quad j = 2, 3, \quad (\text{B1})$$

where L_a is acting on the Hilbert space $\mathcal{H}_a(k_1) \subset \mathcal{H}(k_1)$ defined by $\mathcal{H}_a(k_1) = \{\varphi = \Psi_a \psi \mid \psi \in \mathcal{H}(k_1), \varphi(0) = \varphi(a) = 0\}$. Let $\{\varphi_{a,n} \mid n \in \mathbb{N}\}$ be the set of the eigenfunctions of L_a and $\{\lambda_{a,n} \mid n \in \mathbb{N}\}$ the associated eigenvalues:

$$L_a \varphi_{a,n} = \lambda_{a,n} \varphi_{a,n}, \quad n \in \mathbb{N}. \quad (\text{B2})$$

The expressions of these eigenfunctions and the associated eigenvalues are

$$\varphi_{a,n}: x_1 \mapsto \sqrt{\frac{2}{a}} \Psi_a(x_1) \sin(n\pi x_1/a),$$

$$\lambda_{a,n} = \omega^2 \epsilon_a \mu_0 - k_2^2 - \left(\frac{n\pi}{a}\right)^2. \quad (\text{B3})$$

Note that for $n=0$ the function $\varphi_{a,0}$ is not an eigenfunction of the operator L_a , since it is the null function. We include it because it is more convenient for the following calculations. Developing the components $\hat{E}_{\omega,2}$ and $\hat{E}_{\omega,3}$ on this orthonormal set of eigenfunctions, we obtain from Eq. (B1) the (formal) expression

$$\begin{aligned} \hat{E}_{\omega,j}(x_3) &= \sum_{n \in \mathbb{N}} \varphi_{a,n} \left[\hat{E}_{\omega,j}^{(a,n)}(0) \cos(\sqrt{\lambda_{a,n}} x_3) + (\partial_3 \hat{E}_{\omega,j}^{(a,n)}) \right. \\ &\quad \left. \times (0) \frac{\sin(\sqrt{\lambda_{a,n}} x_3)}{\sqrt{\lambda_{a,n}}} \right], \quad j = 2, 3, \end{aligned} \quad (\text{B4})$$

where the coefficients $\hat{E}_{\omega,j}^{(a,n)}(0)$ and $(\partial_3 \hat{E}_{\omega,j}^{(a,n)})(0)$ are, respectively, the projection the functions $\varphi_{a,n}$ of $\hat{E}_{\omega,j}$ and $\partial_3 \hat{E}_{\omega,j}$,

$$\begin{aligned} \hat{E}_{\omega,j}^{(a,n)}(x_3) &= \int_{[0,d]} dx_1 \varphi_{a,n}(x_1) \hat{E}_{\omega,j}(x_1, x_3), \\ (\partial_3 \hat{E}_{\omega,j}^{(a,n)})(x_3) &= \int_{[0,d]} dx_1 \varphi_{a,n}(x_1) (\partial_3 \hat{E}_{\omega,j})(x_1, x_3), \end{aligned} \quad j = 2, 3, \quad (\text{B5})$$

taken at $x_3=0$.

From Eq. (A7), the electric field satisfies $\nabla \cdot \hat{\mathbf{E}}_\omega = 0$. Then, the expression of the first component $\hat{E}_{\omega,1}$ of the electric field can be deduced from the expression (B4) of the other two components: $\partial_1 \hat{E}_{\omega,1} = -ik_2 \hat{E}_{\omega,2} - \partial_3 \hat{E}_{\omega,3}$. In particular, its x_1 dependence can be developed on the eigenfunctions of the operator

$$L'_a = \omega^2 \epsilon_a \mu_0 - k_2^2 + \partial_1^2 \quad (\text{B6})$$

acting on the Hilbert space $\mathcal{H}'_a(k_1) \subset \mathcal{H}(k_1)$ defined by $\mathcal{H}'_a(k_1) = \{\varphi = \Psi_a \psi \mid \psi \in \mathcal{H}(k_1), (\partial_1 \varphi)(0) = (\partial_1 \varphi)(a) = 0\}$. Let $\{\varphi'_{a,n} \mid n \in \mathbb{N}\}$ be the set of the eigenfunctions of L'_a and $\{\lambda'_{a,n} \mid n \in \mathbb{N}\}$ the associated eigenvalues:

$$L'_a \varphi'_{a,n} = \lambda'_{a,n} \varphi'_{a,n}, \quad n \in \mathbb{N}. \quad (\text{B7})$$

The expressions of these eigenfunctions are

$$\begin{aligned} \varphi'_{a,0}: x_1 \mapsto \sqrt{\frac{1}{a}} \Psi_a(x_1), \\ \varphi'_{a,n}: x_1 \mapsto \sqrt{\frac{2}{a}} \Psi_a(x_1) \cos(n\pi x_1/a), \quad n \in \mathbb{N} \setminus \{0\}. \end{aligned} \quad (\text{B8})$$

Note that the numbering of the eigenfunctions of L_a and L'_a is done such that, for all n in \mathbb{N} , they are associated with the same eigenvalues given by Eq. (B3).

Finally, the modal basis associated with the magnetic field is deduced from Eq. (A7): $\hat{\mathbf{H}}_{\omega} = (\omega\mu_0)^{-1}\nabla_{k_2} \times \hat{\mathbf{E}}_{\omega}$. The x_1 dependence of the component $\hat{H}_{\omega,1}$ can be developed on the eigenfunctions of the operator L_a of Eq. (B3), while the x_1 dependence of the components $\hat{H}_{\omega,2}$ and $\hat{H}_{\omega,3}$ can be developed on the eigenfunctions of the operator L'_a of Eq. (B8).

2. Transfer Matrix in the Modal Basis

We are now ready to obtain the relationship between the vectors $F(0)$ and $F(h)$ in the modal basis and then the transfer matrix. Let the matrices

$$\Phi_{a,n} = \begin{bmatrix} \Phi_{a,n}^{(1)} & 0 \\ 0 & \Phi_{a,n}^{(2)} \end{bmatrix}, \quad \Lambda_{a,n} = \begin{bmatrix} \lambda_{a,n}I & 0 \\ 0 & \lambda_{a,n}I \end{bmatrix}, \quad n \in \mathbb{N}, \quad (\text{B9})$$

be defined from the matrix-valued functions

$$\Phi_{a,n}^{(1)} = \begin{bmatrix} \phi'_{a,n} & 0 \\ 0 & \phi_{a,n} \end{bmatrix}, \quad \Phi_{a,n}^{(2)} = \begin{bmatrix} \phi_{a,n} & 0 \\ 0 & \phi'_{a,n} \end{bmatrix},$$

$$n \in \mathbb{N}, \quad I = \begin{bmatrix} 1 & 0 \\ 0 & 1 \end{bmatrix}. \quad (\text{B10})$$

Then, as with Eq. (B4), it is possible to develop the vector F on the sets of functions and numbers

$$F(x_3) = \sum_{n \in \mathbb{N}} \Phi_{a,n} \left[\cos(\sqrt{\Lambda_{a,n}}x_3)F_{a,n}(0) + \frac{\sin(\sqrt{\Lambda_{a,n}}x_3)}{\sqrt{\Lambda_{a,n}}}(\partial_3 F_{a,n})(0) \right], \quad (\text{B11})$$

where the constant vectors $F_{a,n}(0)$ and $(\partial_3 F_{a,n})(0)$ are, respectively, the projection on the matrix-valued functions $\Phi_{a,n}$ of the vector-valued functions F and $\partial_3 F$,

$$F_{a,n}(x_3) = \int_{[0,d]} dx_1 \Phi_{a,n}(x_1)F(x_1, x_3),$$

$$(\partial_3 F_{a,n})(x_3) = \int_{[0,d]} dx_1 \Phi_{a,n}(x_1)(\partial_3 F)(x_1, x_3), \quad (\text{B12})$$

taken at $x_3=0$. The coefficients $(\partial_3 F_{a,n})(0)$ can be expressed from the coefficients $F_{a,n}(0)$ as follows. After eliminating the vertical components $\hat{E}_{\omega,3}$ and $\hat{H}_{\omega,3}$, Eq. (A7) becomes, for all $0 \leq x_1 \leq a$,

$$\partial_3 F = M_a F, \quad M_a = \begin{bmatrix} -ik_2\sigma_a^{-1}\partial_1 & \sigma_a + \sigma_a^{-1}\partial_1^2 \\ -\sigma_a + k_2^2\sigma_a^{-1} & ik_2\sigma_a^{-1}\partial_1 \end{bmatrix},$$

$$\sigma_a = \omega \begin{bmatrix} 0 & \mu_0 \\ \epsilon_a & 0 \end{bmatrix}. \quad (\text{B13})$$

In this last equation, replacing the vector F by its expression (B11) and then projecting on the functions $\Phi_{a,n}$, one obtains

$$(\partial_3 F_{a,n})(0) = M_{a,n} F_{a,n}(0), \quad p \in \mathbb{N}, \quad (\text{B14})$$

where

$$M_{a,n} = \begin{bmatrix} ik_2(n\pi/a)J\sigma_a^{-1} & [\omega^2\epsilon_a\mu_0 - (n\pi/a)^2]\sigma_a^{-1} \\ -(\omega^2\epsilon_1\mu_0 - k_2^2)\sigma_a^{-1} & ik_2(n\pi/a)J\sigma_a^{-1} \end{bmatrix},$$

$$J = \begin{bmatrix} -1 & 0 \\ 0 & 1 \end{bmatrix}. \quad (\text{B15})$$

Combining expression (B11) of the vector F with the relationship (B14), one obtains the expression of the vector F in all the considered layers from its value at $x_3=0$:

$$F(x_3) = \sum_{n \in \mathbb{N}} \Phi_{a,n} \left[\cos(\sqrt{\Lambda_{a,n}}x_3) + \frac{\sin(\sqrt{\Lambda_{a,n}}x_3)}{\sqrt{\Lambda_{a,n}}} M_{a,n} \right] F_{a,n}(0). \quad (\text{B16})$$

Applying this last expression at $x_3=h$, we obtain the relationship between $F(0)$ and $F(h)$ in the modal basis provided by the transfer matrices $T_{a,n}$:

$$F_{a,n}(h) = T_{a,n} F_{a,n}(0), \quad T_{a,n} = \cos(\sqrt{\Lambda_{a,n}}h) + \frac{\sin(\sqrt{\Lambda_{a,n}}h)}{\sqrt{\Lambda_{a,n}}} M_{a,n}, \quad n \in \mathbb{N}, \quad (\text{B17})$$

where the coefficients $F_{a,n}(h)$ are defined taking Eq. (B12) at $x_3=h$.

3. R Matrix in the Modal Basis

The direct use of the transfer matrix given by Eq. (B17) is known to be numerically unstable [13]. That is the reason the R matrix algorithm based on a rigorous propagation procedure adapted to "elliptic evolution equations" is considered [16]. The R matrix R_a associated with this layer can be defined from a collection of $R_{a,n}$ matrices by

$$\begin{bmatrix} F_{a,n}^{(1)}(h) \\ F_{a,n}^{(1)}(0) \end{bmatrix} = R_{a,n} \begin{bmatrix} F_{a,n}^{(2)}(h) \\ F_{a,n}^{(2)}(0) \end{bmatrix},$$

$$R_{a,n} = \begin{bmatrix} R_{a,n}^{(11)} & R_{a,n}^{(12)} \\ R_{a,n}^{(21)} & R_{a,n}^{(22)} \end{bmatrix} \quad n \in \mathbb{N}. \quad (\text{B18})$$

Their expression can be obtained from the identification of Eqs. (B17) and (B18):

$$R_{a,n}^{(11)} = -[\omega^2\epsilon_a\mu_0 - k_2^2]^{-1} \left[\frac{\cos(\sqrt{\Lambda_{a,n}}h)}{\sqrt{\Lambda_{a,n}}} \frac{\sin(\sqrt{\Lambda_{a,n}}h)}{\sin(\sqrt{\Lambda_{a,n}}h)} \sigma_a + ik_2 \frac{p\pi}{a} J \right],$$

$$R_{a,n}^{(12)} = +[\omega^2\epsilon_a\mu_0 - k_2^2]^{-1} \frac{\sqrt{\Lambda_{a,n}}}{\sin(\sqrt{\Lambda_{a,n}}h)} \sigma_a,$$

$$R_{a,n}^{(21)} = -[\omega^2 \epsilon_a \mu_0 - k_2^2]^{-1} \frac{\sqrt{\lambda_{a,n}}}{\sin(\sqrt{\lambda_{a,n}} h)} \sigma_a,$$

$$R_{a,n}^{(22)} = -[\omega^2 \epsilon_a \mu_0 - k_2^2]^{-1} \left[\frac{\cos(\sqrt{\lambda_{a,n}} h)}{\sin(\sqrt{\lambda_{a,n}} h)} \sigma_a - i k_2 \frac{p \pi}{a} \mathbf{J} \right]. \quad (\text{B19})$$

We have here an expression of the R matrix associated with each layer considered in the modal basis.

APPENDIX C: SOLUTION OF MAXWELL'S EQUATIONS IN A HOMOGENEOUS LAYER

The Fourier basis can be considered as the modal basis associated with a homogeneous layer [15]. Then the solution of Maxwell's equations in this homogeneous layer can be written as the expression of Eq. (B16):

$$F(x_3 + h) = \sum_{p \in \mathbf{Z}} \Phi_{0,p} \left[\cos(\sqrt{\Lambda_{0,p}} x_3) + \frac{\sin(\sqrt{\Lambda_{0,p}} x_3)}{\sqrt{\Lambda_{0,p}}} M_{0,p} \right] F_{0,p}(h), \quad (\text{C1})$$

where $\Phi_{0,p}$ is the tensor product of the 4×4 unit matrix with the plane-wave function

$$\phi_{0,p} : x_1 \mapsto \sqrt{\frac{1}{d}} \exp[i(k_1 + p 2\pi/d)x_1], \quad p \in \mathbf{Z}, \quad (\text{C2})$$

$\Lambda_{0,p}$ is the product of the 4×4 unit matrix with the eigenvalue

$$\lambda_{0,p} = \omega^2 \epsilon_0 \mu_0 - k_2^2 - \left(k_1 + p \frac{2\pi}{d} \right)^2, \quad (\text{C3})$$

and the matrix $M_{0,p}$ is defined by

$$M_{0,p} = \begin{bmatrix} k_2(k_1 + p 2\pi/d) \sigma_0^{-1} & [\omega^2 \epsilon_0 \mu_0 - (k_1 + p 2\pi/d)^2] \sigma_0^{-1} \\ -(\omega^2 \epsilon_0 \mu_0 - k_2^2) \sigma_0^{-1} & -k_2(k_1 + p 2\pi/d) \sigma_0^{-1} \end{bmatrix} \quad (\text{C4})$$

from the constant 2×2 matrix

$$\sigma_0 = \omega \begin{bmatrix} 0 & \mu_0 \\ \epsilon_0 & 0 \end{bmatrix}. \quad (\text{C5})$$

The constant vectors $F_{0,p}(h)$ are the Fourier coefficients of the vector $F(h)$, i.e., the projection on the matrix-valued functions $\Phi_{0,p}$ of the vector-valued function F

$$F_{0,p}(x_3) = \int_{[0,d]} dx_1 \overline{\Phi_{0,p}(x_1)} F(x_1, x_3) \quad (\text{C6})$$

taken at $x_3 = h$.

Finally, the R matrix R_0 associated with this homogeneous layer can be defined from a collection of $R_{0,p}$ matrices by

$$\begin{bmatrix} F_{0,p}^{(1)}(h_0 + h) \\ F_{0,p}^{(1)}(h) \end{bmatrix} = R_{0,p} \begin{bmatrix} F_{0,p}^{(2)}(h_0 + h) \\ F_{0,p}^{(2)}(h) \end{bmatrix},$$

$$R_{0,p} = \begin{bmatrix} R_{0,p}^{(11)} & R_{0,p}^{(12)} \\ R_{0,p}^{(21)} & R_{0,p}^{(22)} \end{bmatrix}, \quad p \in \mathbf{Z}, \quad (\text{C7})$$

with their expression provided by

$$R_{0,p}^{(11)} = -[\omega^2 \epsilon_0 \mu_0 - k_2^2]^{-1} \left[\frac{\cos(\sqrt{\lambda_{0,p}} h_0)}{\sin(\sqrt{\lambda_{0,p}} h_0)} \sigma_0 - k_2 \left(k_1 + p \frac{2\pi}{d} \right) I \right],$$

$$R_{0,p}^{(12)} = +[\omega^2 \epsilon_0 \mu_0 - k_2^2]^{-1} \frac{\sqrt{\lambda_{0,p}}}{\sin(\sqrt{\lambda_{0,p}} h_0)} \sigma_0,$$

$$R_{0,p}^{(21)} = -[\omega^2 \epsilon_0 \mu_0 - k_2^2]^{-1} \frac{\sqrt{\lambda_{0,p}}}{\sin(\sqrt{\lambda_{0,p}} h_0)} \sigma_0,$$

$$R_{0,p}^{(22)} = -[\omega^2 \epsilon_0 \mu_0 - k_2^2]^{-1} \left[\frac{\cos(\sqrt{\lambda_{0,p}} h_0)}{\sin(\sqrt{\lambda_{0,p}} h_0)} \sigma_0 + k_2 \left(k_1 + p \frac{2\pi}{d} \right) I \right]. \quad (\text{C8})$$

ACKNOWLEDGMENTS

This work was partly supported by the research program METAPHORE (Action Concertée nanosciences et nanotechnologies of the French Ministère de la Recherche et des Nouvelles Technologies) as well as Thales Alenia Space.

REFERENCES

1. L. C. Botten, M. S. Craig, R. C. McPhedran, J. L. Adams, and J. R. Andrewartha, "The dielectric lamellar diffraction grating," *Opt. Acta* **28**, 413–428 (1981).
2. L. C. Botten, M. S. Craig, R. C. McPhedran, J. L. Adams, and J. R. Andrewartha, "The finitely conducting lamellar diffraction grating," *Opt. Acta* **28**, 1087–1102 (1981).
3. L. C. Botten, M. S. Craig, and R. C. McPhedran, "Highly conducting lamellar diffraction grating," *Opt. Acta* **28**, 1103–1106 (1981).
4. M. G. Moharam and T. K. Gaylord, "Rigorous coupled-waves analysis of metallic surface-relief grating," *J. Opt. Soc. Am. A* **3**, 1780–1787 (1986).
5. T. W. Ebbesen, H. J. Lezec, H. F. Ghaemi, T. Thio, and P. A. Wolff, "Extraordinary optical transmission through subwavelength hole arrays," *Nature (London)* **391**, 667–669 (1998).
6. S. Enoch, M. Nevière, E. Popov, and R. Reinisch, "Enhanced light transmission by hole arrays," *J. Opt. A, Pure Appl. Opt.* **4**, S83–S87 (2002).
7. S. Enoch, G. Tayeb, P. Sabouroux, N. Guérin, and P. Vincent, "A metamaterial for directive emission," *Phys. Rev. Lett.* **89**, 213902 (2002).
8. P. Andrew and W. L. Barnes, "Molecular fluorescence above metallic gratings," *Phys. Rev. B* **64**, 125405 (2001).

9. J. Kalkman, C. Strohhöfer, B. Gralak, and A. Polman, "Surface plasmon polariton modified emission of erbium in a metallodielectric grating," *Appl. Phys. Lett.* **83**, 30 (2003).
10. Y. De Wilde, F. Formanek, R. Carminati, B. Gralak, P.-A. Lemoine, K. Joulain, J.-P. Mulet, Y. Chen, and J.-J. Greffet, "Thermal radiation scanning tunnelling microscopy," *Nature (London)* **444**, 740–743 (2006).
11. M. C. K. Wiltshire, J. B. Pendry, I. R. Young, D. J. Larkman, D. J. Gilderdale, and J. V. Hajnal, "Microstructured magnetic materials for RF flux guides in magnetic resonance imaging," *Science* **291**, 849–851 (2001).
12. R. A. Shelby, D. R. Smith, and S. Schultz, "Experimental verification of a negative index of refraction," *Science* **292**, 77–79 (2001).
13. L. Li, "Formulation and comparison of two recursive matrix algorithms for modeling layered diffraction gratings," *J. Opt. Soc. Am. A* **13**, 1024–1035 (1996).
14. S. Campbell, L. C. Botten, C. Martijn De Sterke, and R. C. McPhedran, "Fresnel formulation for multi-element lamellar diffraction gratings in conical mountings," *Waves Random Complex Media* **17**, 455–475 (2007).
15. L. Li, "A modal analysis of lamellar diffraction gratings in conical mountings," *J. Mod. Opt.* **40**, 553–573 (1993).
16. B. Gralak, M. de Dood, G. Tayeb, S. Enoch, and D. Maystre, "Theoretical study of photonic band gaps in woodpile crystals," *Phys. Rev. E* **67**, 066601 (2003).
17. Z.-Y. Li and K.-M. Ho, "Analytic modal solution to light propagation through layer-by-layer metallic photonic crystals," *Phys. Rev. B* **67**, 165104 (2003).
18. G. Tayeb and S. Enoch, "Combined fictitious sources–scattering matrix method," *J. Opt. Soc. Am. A* **21**, 1417–1423 (2004).
19. C. Hafner, *The Generalized Multipole Technique for Computational Electromagnetics* (Artech House, 1990).
20. G. Tayeb, "The method of fictitious sources applied to diffraction gratings," Special issue on Generalized Multipole Techniques (GMT) of Applied Computational Electromagnetics Society Journal 9, 90–100 (1994).
21. D. Maystre, M. Saillard, and G. Tayeb, *Scattering* (Academic, 2001).
22. D. Kaklamani and H. Anastassiou, "Aspects of the method of auxiliary sources (MAS) in computational electromagnetics," *IEEE Antennas Propag. Mag.* **44**, 48–64 (2002).
23. G. Benelli, S. Enoch, and G. Tayeb, "Modelling of a single object embedded in a layered medium," *J. Mod. Opt.* **54**, 871–879 (2007).